Astron. Astrophys. 356, 827–839 (2000)

ASTRONOMY AND ASTROPHYSICS

A detailed study of the ringed galaxy NGC 3344⋆

L. Verdes-Montenegro[1], **A. Bosma**[2], **and E. Athanassoula**[2]

[1] Instituto de Astrofísica de Andalucía, CSIC, Apdo. 3004, 18080 Granada, Spain
[2] Observatoire de Marseille, 2 Place le Verrier, 13248 Marseille Cedex 4, France

Received 6 December 1999 / Accepted 18 February 2000

Abstract. We study the relatively isolated galaxy NGC 3344, classified as SABbc, as part of our study of ringed isolated non-barred galaxies. This galaxy shows an inner and an outer ring, together with a small bar inside the inner ring. This bar is too small to relate it directly to the formation of the outer ring and we explore here its origin through HI (WSRT) line data together with broad band BR CCD-photometry and optical spectroscopy.

We show that the bar is exponential and dominates the central parts, while the bulge component is small. This suggests a morphological type later than Sbc for NGC 3344, further supported by the strong abundance gradient reported in the literature for this galaxy. The inner ring defines the beginning of the spiral structure which partially wraps around this ring at small radii. Less than 1% of the HI is located in this ring which is mostly composed by a young stellar population.

The outer ring shows colours similar to those of the inner ring, indicating that is actively forming stars. It is not located symmetrically with respect to the center of the galaxy, its center being shifted by about 18″. Twenty percent of the HI emission is concentrated in this ring.

The atomic gas is distributed asymmetrically in NGC 3344, extending 20% farther to the SE than in the opposite direction. The outer parts of the velocity field also deviate from that of a disk in circular rotation, with a pronounced warp especially abrupt to the SE.

We derive a mass model for this galaxy, but the deviations from axisymmetry prohibit a good determination of a single pattern speed explaining the location of the rings.

Key words: galaxies: individual: NGC 3344 – galaxies: kinematics and dynamics – galaxies: photometry – galaxies: spiral – galaxies: structure

1. Introduction

Rings and pseudorings are mainly observed in barred disk galaxies, mostly of early type (cf. Buta 1995). Schwarz (1981), using "sticky particle" simulations, showed that they form naturally by the response of a gaseous disk to a rotating non-axisymmetric mass distribution, and are linked to resonances. The latter is corroborated by statistical analyses (e.g. Athanassoula et al. 1982; Schwarz 1984a,1984b,1984c,1985; Buta 1986; Buta & Crocker 1991) based on catalogues of ring dimensions (e.g. De Vaucouleurs & Buta 1980). The association of rings with resonant features leads, when combined with the rotation curve, to an estimate of the pattern speed of the structure (see e.g. Elmegreen 1996 for a discussion on the different methods used for pattern speed determinations).

Non-barred isolated galaxies with rings, in which a priori no feature exists to set up the pattern speed and therefore the resonances, are particularly intriguing. In two previous papers we presented HI observations, CCD imaging and spectroscopy of the galaxies NGC 7217 (Verdes-Montenegro et al. 1995) and NGC 6015 (Verdes-Montenegro et al. 1997). In NGC 7217 the three main types of rings possible in barred galaxies are present and their location consistent with that of resonances due to a single bi-symmetric pattern. Nevertheless, the feature responsible for setting up this pattern could not be identified, and we discussed elsewhere (cf. Athanassoula 1996; Athanassoula et al. 1996) scenarios in which a bar was present in this galaxy, but disappeared e.g. due to an increase in the central concentration of the galaxy, thereby leaving the rings, and creating a retrograde population of stars which is indeed observed in this galaxy (cf. Merrifield & Kuijken 1994). In the case of NGC 6015, assuming that the outer ring is at the outer Lindblad resonance, we find that the end of the inner spiral structure is located at the ultraharmonic (4:1) resonance, in agreement with the result found by Patsis et al. (1994).

In this paper we continue the study of non-barred isolated galaxies with rings, in order to shed light on the formation process of these rings. We report results from the analysis of the optical and HI line emission and Hα spectroscopy of NGC 3344, a ringed and relatively isolated galaxy which presents a bar too small to be related with the formation of the outer ring at the location of the outer Lindblad resonance of the bar (Athanassoula et al. 1982). Due to the small size of the bar this galaxy was classified as non-barred in the RC2 catalog (1976), but in the RC3 catalog (1991) it is given as (R)SAB(r)bc. Martin (1995) measured the bar to have low ellipticity (semiaxes of 12″ × 10″) from the optical image in the Sandage & Bedke (1988)

Send offprint requests to: L. Verdes-Montenegro

⋆ based partially on data collected at the Observatoire de Haute Provence, France

atlas. The main parameters of NGC 3344 are listed in Table 1. De Vaucouleurs & Buta (1980) report the existence of an inner and an outer ring with diameters of $\sim 54'' \times 51''$ and $360'' \times 360''$ respectively. They also note the existence of a distinct nucleus $3'' \times 3''$ in size, common among barred spirals. It has been recently classified as an HII nucleus by Maoz et al. (1996) from HST UV imaging. The inner ring is coincident with a CO peak (Braine et al. 1993). NGC 3344 shows a spiral structure, analysed by Considère & Athanassoula (1988).

The total HI emission of NGC 3344 has been measured by Staveley-Smith & Davies (1987) with a $36'$ beam. Single dish HI mapping was done by Corbelli et al. (1989) (beam $\simeq 3'.9$) who report peculiar kinematics with sharp changes, a behaviour later interpreted by Briggs (1990) as due to a warp occurring in an almost face-on galaxy.

The systemic heliocentric radial velocity of this galaxy, obtained from our HI data and corrected to the centroid of the Local Group is 586.8 km s^{-1}. A Hubble constant of 75 km s^{-1} Mpc^{-1} gives a distance of 6.9 Mpc. We have studied the neighborhood of NGC 3344 within 1 Mpc and 500 km s^{-1}. From the NED[1] database we find that the nearest bright galaxy is NGC 3274 at an apparent separation of 3.7 degrees (projected separation of 446 kpc at the distance of NGC 3344), a velocity of 537 km s^{-1} and 2 mag fainter. The next galaxy is UGC 5672, 4.2 degrees away from NGC 3344 (506 kpc), with a velocity of 531 km s^{-1} and 3 mag fainter. The CfA redshift survey indicates the existence of six dwarf galaxies within the same area, without measured redshift and 4 mag fainter than NGC 3344.

Table 1. Parameters of NGC 3344.

Center position[a]	
α(1950.0)	$10^h\ 40^m\ 46.^s92$
δ(1950.0)	$25^\circ\ 11'\ 07.''61$
Inclination	25.5$^{\circ,b}$
	34$^{\circ,c}$, 24$^{\circ,d}$, 15$^{\circ,e}$, 20.5$^{\circ,f}$
Position angle	-23.9$^{\circ,b}$
	-12$^{\circ,c}$, -5$^{\circ,d}$, -52$^{\circ,e}$
B_T[b]	10.4
B_T^o[b]	10.3
R_{25}[b]	$210.6''$ (9.2 kpc)
HI systemic heliocentric velocity (km s^{-1})	586.8[b],583.3[g]
Distance[b]	6.9 Mpc

[a] Central position of NGC 3344 obtained from our B image.
[b] This paper.
[c] García-Gómez & Athanassoula (1991).
[d] Grosbøl (1985).
[e] Considère & Athanassoula (1988).
[f] Briggs (1990).
[g] Staveley-Smith & Davies (1987).

2. Observations and data analysis

2.1. Photometry

We have used optical images in the B_J and R bands of the photometric system by Gullixson et al. (1995) from the Catalog of digital images elaborated by Frei et al. (1996). The images were taken with the 1.1 m telescope of Lowell Observatory with a RCA CCD camera of 326×512 pixels and an exposure time of 300s in each filter. Details of the reduction and calibration of the data as well as star removal can be found in Frei et al. The errors in the sky determination were 6% in B and 3% in R. Colours have been corrected for galactic absorption using the extinction value given by Burstein & Heiles (1984), with the reddening law from Savage & Mathis (1979), and, for internal extinction, with $A_i = 0.07$ obtained from the inclination derived in this paper for NGC 3344 with the definition in de Vaucouleurs et al. (1991). In order to calculate the scale, orientation and absolute coordinates of the frame we have measured the centroid of the stars in the field from the original images kindly provided by Z. Frei. By using the CCMAP routine from IRAF[2] package we find a scale of $1.''36$/pixel, and the frame is in the N–S/E–W direction with an error of 0.3 degrees. The center of NGC 3344 in the B band is located at α(1950.0) = $10^h\ 40^m\ 46.^s92$ and δ(1950.0) = $25^\circ\ 11'\ 07.''61$, coincident with the one of the R image within $0.''3$. We estimate that our positions are good to within $0.''1$ as obtained from the standard deviation of the centroid of the field stars. The seeing of each frame amounts to $4.''1$ in B and $3.''1$ in R. The orientation of all the images shown in this paper is North up and East to the left, while offset positions are in arcsec relative to the center of the galaxy in the B band.

2.2. Optical spectroscopy

Long slit spectra at position angles 156°, 136°, and 176°, centered on the nucleus, around the wavelength range of the Hα and [NII] lines, have been obtained in February 1998 with the 1.93m telescope of the Observatoire de Haute Provence, using the Carelec spectrograph equipped with a Tektronix CCD camera with 512x512 pixels. The data were reduced in a standard manner, and radial velocities were determined from the Hα-line, the [NII]-lines and the [SII]-lines. Using the best fit for the spatial orientation parameters in the inner regions as determined from the 21-cm line observations (see Sect. 3.3), these radial velocities were converted into circular velocities, and an average was made from the results at either side of the center. These circular velocities were adopted later (cf. Sect. 4) as representative for the inner parts of the rotation curve.

2.3. Radio observations

We have observed NGC 3344 in the 21 cm line of HI with the Westerbork Synthesis Radio Telescope (WSRT[3]) in 1983. We

[1] The NASA/IPAC extragalactic database (NED) is operated by the Jet Propulsion Laboratory, California Institute of Technology, under contract with the National Aeronautics and Space Administration

[2] IRAF is distributed by National Optical Astronomy Observatories which are operated by the Association of Universities for Research in Astronomy, Inc., under contract to the National Science Foundation.

[3] The Westerbork Synthesis Radio Telescope is operated by the Netherlands Foundation for Radio Astronomy with financial support

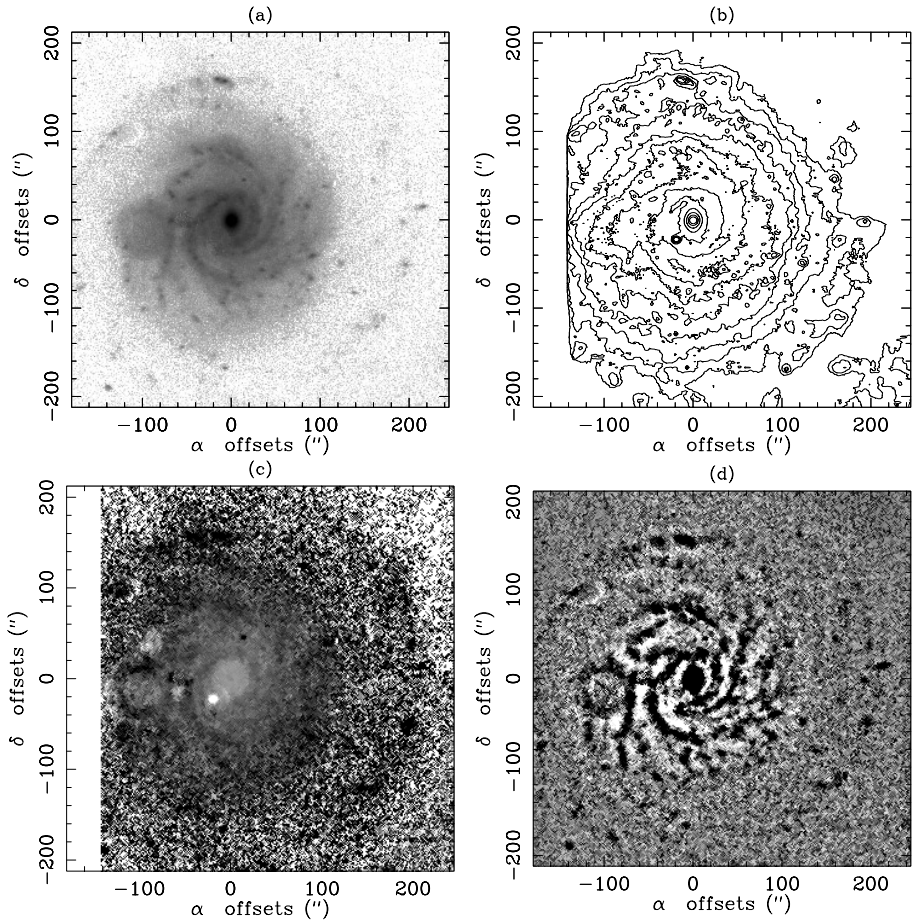

Fig. 1. a B image of NGC 3344 in a logarithmic grey scale representation. Higher intensities are darker. **b** Isophotal contours corresponding to the R filter image, ranging from 18.8 to 24.8 mag arcsec^{-2}, with a step of 0.5 mag arcsec^{-2}. **c** B–R colour image in a grey scale where black is bluer and white is redder. Colours have been corrected for interstellar absorption as explained in Sect. 2.1. **d** Sharpening of the B image shown in Fig. 1a obtained by the subtraction of a $15'' \times 15''$ box median filtered image. Darker areas correspond to excess emission. The orientation of all the images is North up and East to the left.

used 40 interferometers with spacings ranging from 54 m to 2718 m in steps of 72 m. This results in a synthesized beam of $13\farcs3 \times 30\farcs5$ ($\alpha \times \delta$) and first grating response at $10' \times 23'$ ($\alpha \times \delta$). We used a digital backend (Bos et al. 1981) resulting in 31 channel maps at heliocentric velocities 466.4 to 713.6 km s^{-1}. Hanning smoothing was applied on-line, giving a velocity resolution of twice the channel spacing of 8.2 km s^{-1}.

The data were edited and calibrated as explained in Verdes-Montenegro et al. (1995). A rms noise level of ~ 1.3 mJy/beam was achieved after 12 hours of integration. In order to get a higher signal-to-noise ratio in the integrated HI distribution and associated radial velocity field, we convolved the map data with a gaussian, leading to a beam size of $60\farcs0 \times 60\farcs0$ ($\alpha \times \delta$) and rms of 0.4 mJy/beam. Primary beam corrections have been applied to our maps.

3. Results

3.1. Optical emission

The B band image of NGC 3344 is shown in Fig. 1a in a logarithmic greyscale representation. Residuals from a star removal are still apparent there. Isophotal contours of the R band are presented in Fig. 1b and show clearly the existence of an inner small bar or oval. The corresponding colour index image B–R is given in Fig. 1c. The outer parts of the galaxy were only partially covered to the east, and we have complemented our analysis with a film copy of the original plate obtained for the RSA catalog, kindly provided by Sandage to Considère & Athanassoula (1988). As can be seen in Fig. 1a this galaxy shows a well defined spiral structure, that appears enhanced in the "sharpened" image obtained by the subtraction of a $15'' \times 15''$ median filtered B image (Fig. 1d). It is dominated by a two arm main component that is stronger for the inner $100''$ and extends with gaps up to a radius of $180''$ from the center, as found by Considère & Athanassoula (1988) through a Fourier analysis of the light distribution. One of the arms seems to end in the western part of the outer pseudoring structure. Other small arms exist as bifurcations of the main ones starting at $\sim 50''$ and are well described by m=5 and m=6 components. The outer pseudoring appears faint and narrow relative to the size of the galaxy (cross section $\sigma \sim 15'' - 25''$, $\sigma/D_{25} \sim 0.03 - 0.06$), and can be better traced in the B band as blue knots extending from $115^\circ \leq$ p.a. $\leq 325^\circ$, with a smoother distribution in the B–R colour index image. In Table 2 we list the geometrical parameters of the pseudoring obtained through fitting an ellipse, together with characteristic colour indices. Corrected colour indices – $(B\text{-}R)_{o,corr}$ – have been calculated by subtraction of the subjacent disk population to the B and R bands, obtained through interpolation between

from the Netherlands Foundation for the Advancement of Pure Research (Z. W. O.)

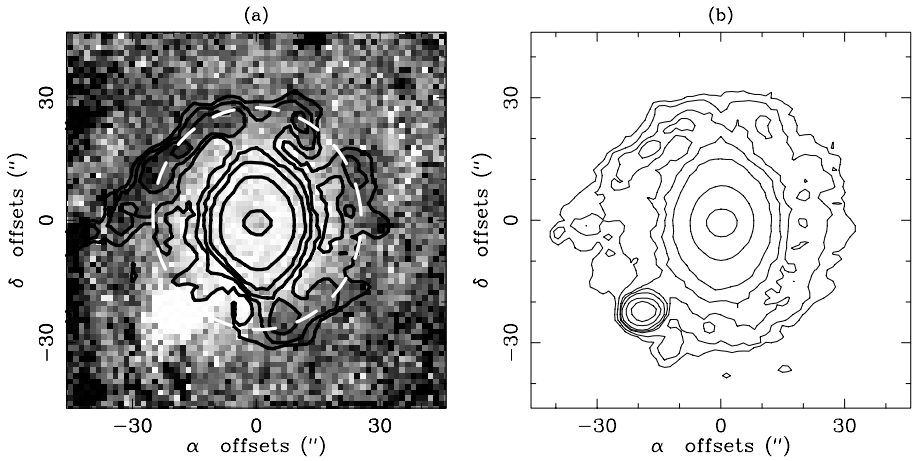

Fig. 2a and b. Close up of the central region of NGC 3344. **a** B–R colour image in a grey scale where black is bluer and white is redder with overlapped isophotal contours corresponding to the B band image with values 19.1, 20.7, 21.0, 21.2, 21.3 and 21.4 mag arcsec^{-2}. **b** Isophotal contours corresponding to the R filter image with values 18.1, 19.3, 19.9, 20.1, 20.2, 20.4 and 20.5 mag arcsec^{-2}. The orientation of all the images is North up and East to the left.

Table 2. Ring and bar parameters[a]

Feature	Semimajor axis (″)	Semiminor axis (″)	Pos. angle (°)	B–R	$(B–R)_o$	$(B–R)_{o,corr}$
Bar	19.5	14.5	0.8	1.17 ± 0.02	1.13	–
Inner ring	27.2	25.2	7.3	0.95 ± 0.10	0.91	0.52
Outer ring	196.9	180.0	-22.9	0.42 ± 0.32	0.38	0.40

[a] Typical rms before fit is 15″ and 2″ after.

radii inside and outside each ring. A similar correction was not feasible for the bar due to its mixing with the bulge. After the correction both inner and outer rings have very similar blue colours.

Both the bar and the inner ring, wrapping around the bar, are clearly seen in the close-up of the inner part of NGC 3344 shown in Fig. 2a. Here the B band contours are overlayed to a greyscale representation of the B–R colour index image, showing that the inner ring is bluer than the bar (cf. also Table 2). The inner ring appears in the B band as made partly of the wrapped spiral arms and extends from $-170° \leq$ p.a. $\leq 75°$. It is not continuous, but shows several knots with a typical thickness of 8″ embedded in a smoother distribution, being weaker in R band (Fig. 2b). Its dimensions as found from our B image (Table 2) are nearly the same as measured by de Vaucouleurs & Buta (1980). The size and orientation of the bar were obtained from the R image, less contaminated by the spiral arms. The position angle of the bar in the deprojected image of the galaxy is 24°. We obtain for it a larger size and ellipticity than measured by Martin (1995), whose measurement refers to a photographic plate in the blue.

Fig. 3 shows the radial brightness profiles for NGC 3344 in the two filters as a function of the equivalent radius (r^*, defined as the radius of a circle having the same area as that delimited by the isophote) of the corresponding isophotal level. Radii are limited to r^* = 170″ in B and 135″ in R bands by the edge of the frame, so that the outer ring could not be reached. The signature of the bar is visible in the central parts ($r^* \leq 19''$) as a pronounced steepness. The inner ring is visible for $r^* \sim 19''$ to 32″ being more prominent in the B band, and almost not present

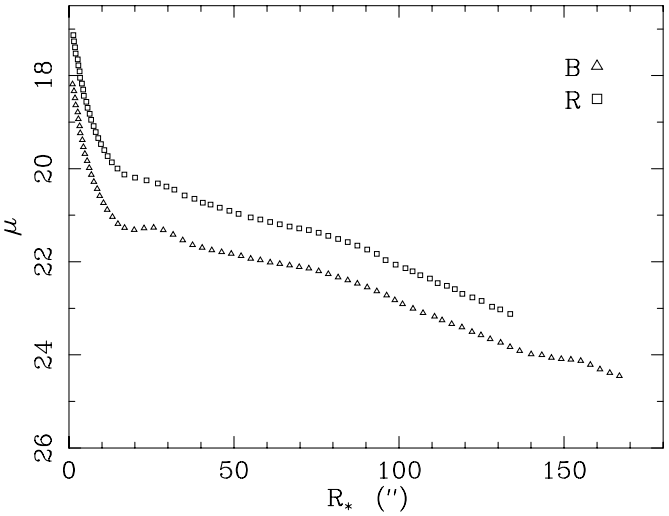

Fig. 3. Averaged radial profiles in each individual photometric pass band as a function of the equivalent radius of each isophotal level.

in the R band profile. The brightest parts of the spiral structure are found between r^* = 60″ and 100″ with some bright HII regions between 145″ and 165″ nearly at the edge of the frame. B and I profiles extending to radii larger than allowed by our data were kindly provided by D. and B. Elmegreen, based on their work using plates (Elmegreen & Elmegreen 1984). The outer ring is only visible in the blue light coming from young stars but not in the older population traced by the I band emission. The same holds for the inner ring.

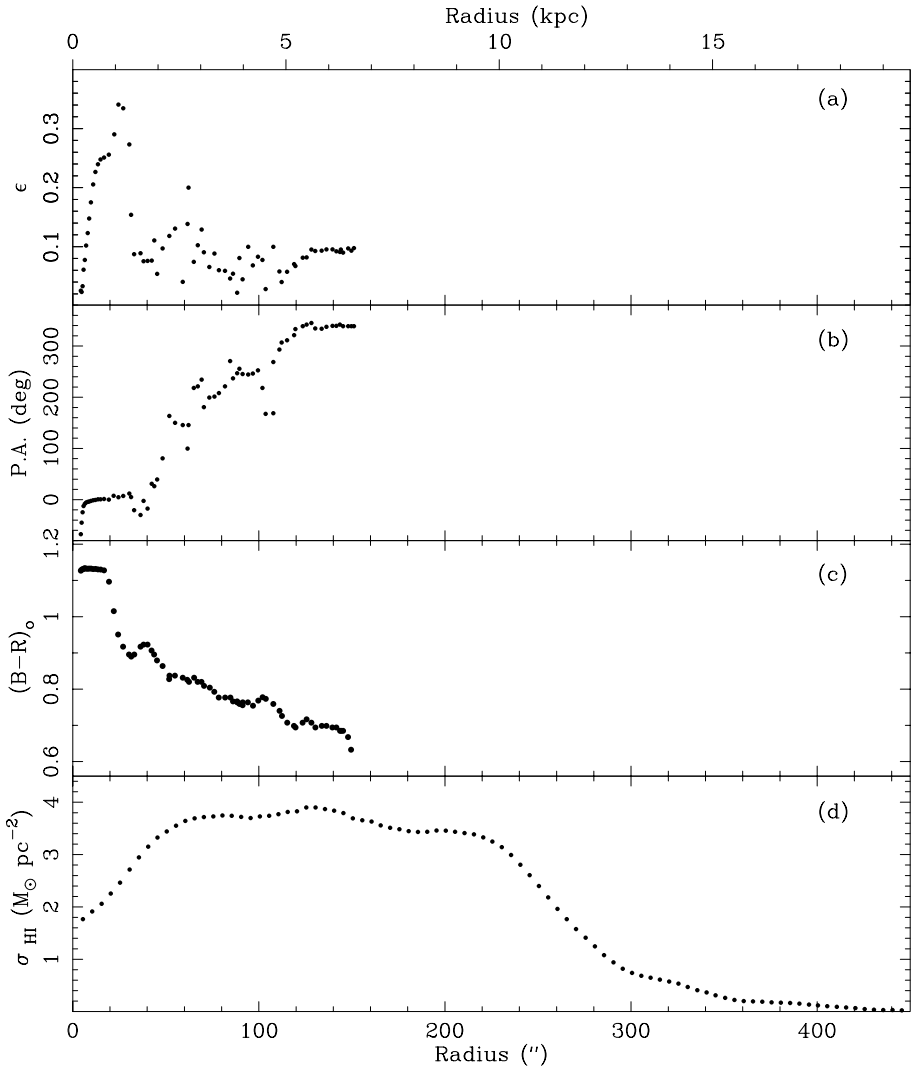

Fig. 4a–d. Ellipticity (**a**), position angle (**b**) of the ellipses fitted to the R isophotes as a function of their semimajor axis length (see Sect. 3.1). **c** Radial colour index profiles $(B–R)_0$ corrected as explained in Sect. 2.1 and obtained by integrating the corresponding image in elliptic annuli of 3″ width and with the geometrical parameters corresponding to the R isophotes. Angles are measured from N to E. **d** The same as **c** for the HI surface density. The lower radial scale is in arcsec and the upper one in kpc, for D = 6.9 Mpc.

Ellipticities (ϵ) and position angles (p.a.) of the ellipses fitted to the isophotes in the R band are shown in Fig. 4a and b respectively. Fig. 5 illustrates these variations with selected isophotes together with the corresponding fitted ellipses and major axes. The spiral structure has also been outlined in this figure to show its effect on the p.a. determination. In the innermost parts ϵ is close to 0 as expected because of the nucleus/bulge component. There the p.a. reaches a nearly constant value, since the presence of the spheroidal component decreases the axial ratio of the bar, without affecting its orientation. From 6″ to 19″ the isophotes are almost self-similar, with the position angle changing slightly from p.a. $\sim$ –8° to 1°. It is suggestive of a little twisting of the bar, and this occurs in the same sense as the spiral structure (Fig. 5a). The ellipticities grow rapidly to reach a plateau of 0.25 – 0.26 between 15″ and 19″, a clear signature of the small bar component, and then goes down to about 30″ where the disk component becomes dominant. The inner ring can be only distinguished from the adjacent areas by its larger brightness, specially in B band, while keeping similar orientation and ellipticity as the nearby isophotes.

The radius range from 30″ – 110″ is heavily affected by the spiral structure and there ellipses are a poor approximation to isophote shapes (Fig. 5b-d). The corresponding values of the ellipticities are very noisy yet follow an overall trend that connects reasonably well with the outer disk, much less perturbed by the spiral arms. The same is true for the p.a. whose values are heavily influenced by the spiral structure as seen in Fig. 5b-d.

Since the spiral structure is weaker in the outer parts, the outer isophotes of NGC 3344 are well represented by ellipses, and their p.a. and ϵ are well defined. Thus between 130″ and 150″ the values are p.a. = –20.2° $\pm$ 1.6° and ϵ of 0.094 $\pm$ 0.002. With the assumption that these outer isophotes are intrinsically circular, and therefore representative of a pure disk component, the galaxy would have an inclination to the line of sight of 25.5° $\pm$ 0.4° (formal error).

The center of the isophotes for radii $<$ 20″ are coincident with the photometric maximum to within 1″. From 20″ to 110″ these centers are badly defined, just like the orientation of the isophotes. We can again follow them between 110″ and 150″ where they show a drift in the SE direction so that the center

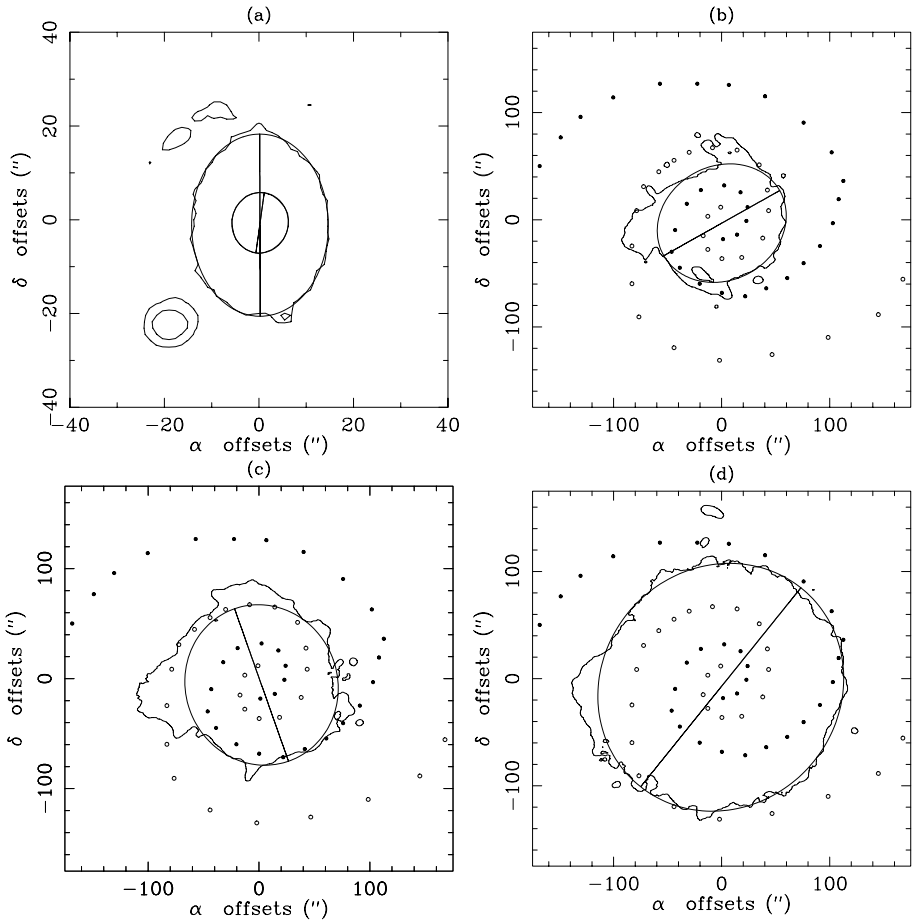

Fig. 5. a Isophotes of the R band image for the bar of NGC 3344 at radii 6″ and 19″. The fitted ellipses and corresponding major axis are plotted showing a small change in the position angle ($\sim 10^{\circ}$). **b–d** The same as in **a** for radii 62″, 73″ and 119″, respectively. The open and filled dots trace the two main spiral arms. A change in p.a. can be noticed from **b** to **d** in agreement with the form of the spiral structure.

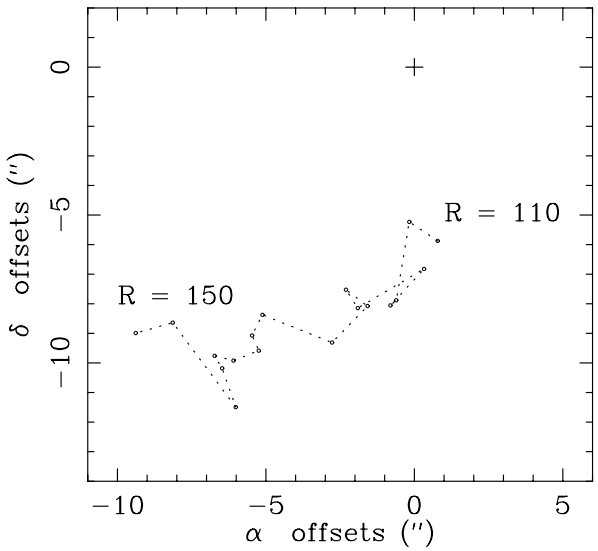

Fig. 6. Position of the centers of the R isophotes from radius = 110″ to 150″, showing a drift with increasing radius of $\sim 11''$ to the SE.

of the isophotes shifts continuously from offset (0,–5)″ to (–6,–11)″, and hence by $\sim 8''$ (Fig. 6).

The radial colour index profile (Fig. 4c) has been calculated from the individual B and R bands as follows. The images have been integrated over circular annuli with thickness of 3″ on the deprojected image of the galaxy. The adopted parameters for radii smaller than 20″ and larger than 110″ were those corresponding to the fitted isophotes (Fig. 4 a and b). For the intermediate area we obtained isophotal parameters by applying sliding means to the ellipticities and position angles in this region. We have then obtained the corresponding B–R colour indices, and corrected them as explained in Sect. 2.1. The bar is clearly seen over all its extension (radius $\leq 19''$) as the reddest part of NGC 3344. The inner ring appears as a dip in the profile. Other blue humps are superimposed onto a redder curve at radii $\sim 50''$, 120″ plus one at the edge of the profile, all associated with features in the spiral structure.

3.2. Atomic gas distribution

In Fig. 7 we display the channel maps containing the HI emission at the indicated heliocentric velocities, produced with a beam of $13\farcs2 \times 30\farcs5$. Each channel has a width of 8.2 km s^{-1} and an rms noise of 1.9 K, implying a level of 2.9×10^{19} at cm^{-2}. The HI distribution shows an asymmetry between the low and high velocity channels, extending farther in the SE half than in the NW one. For radii up to $\sim 2\farcm7$ NGC 3344 shows a characteristic pattern of circular rotation, while for larger radii non circular motions clearly exist. The contours in the western

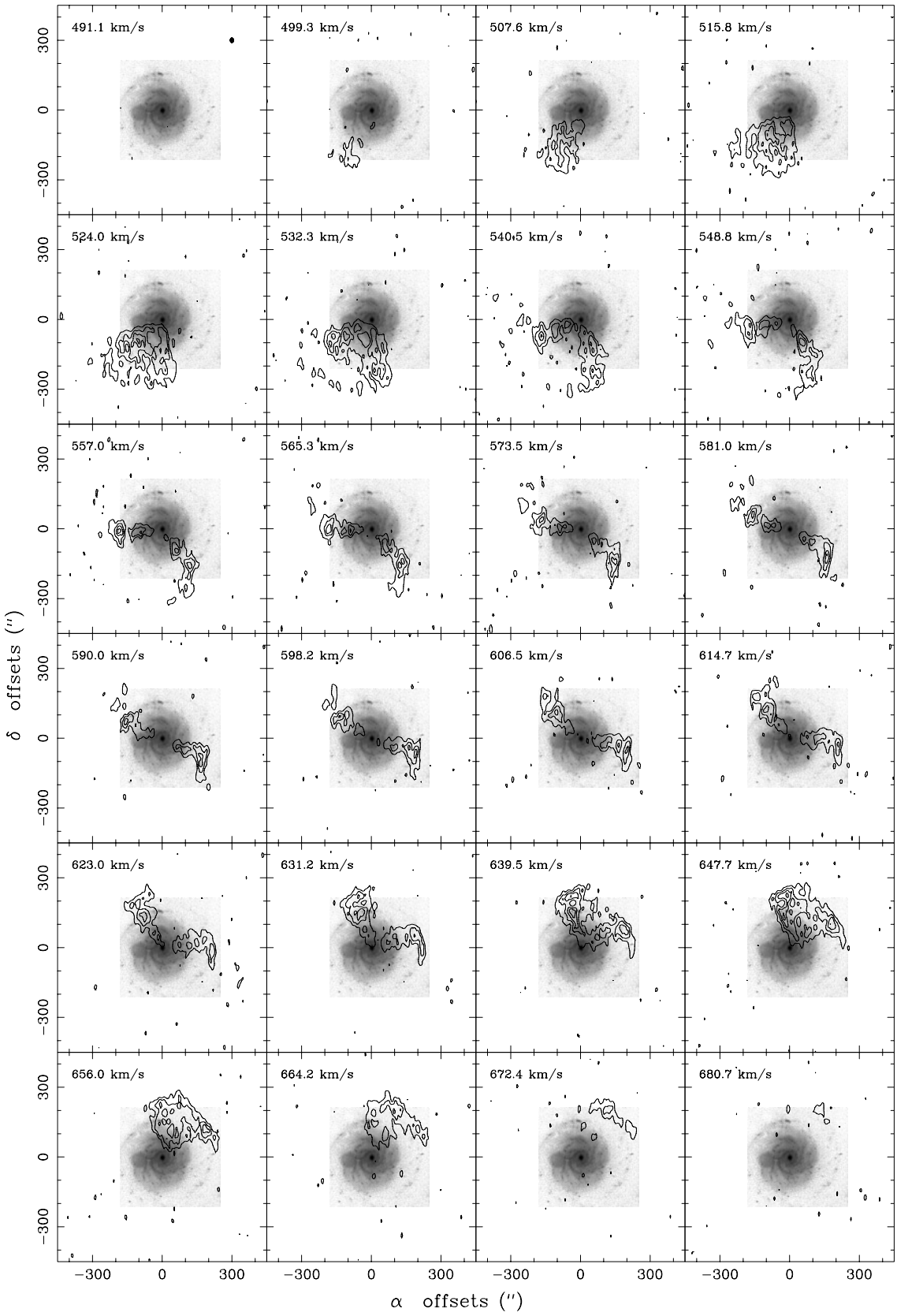

Fig. 7. Channel maps of the 21 cm line radiation superimposed on the B image. The heliocentric velocities are as indicated in each panel. Contours correspond to -6.6, 6.6, 13.3, 20.0, 26.6, 33.3 and 39.9 K, and the rms noise of the maps is 1.9 K. The synthesized beam ($13\farcs3 \times 30\farcs5$ – $\alpha \times \delta$) is plotted in the upper left panel.

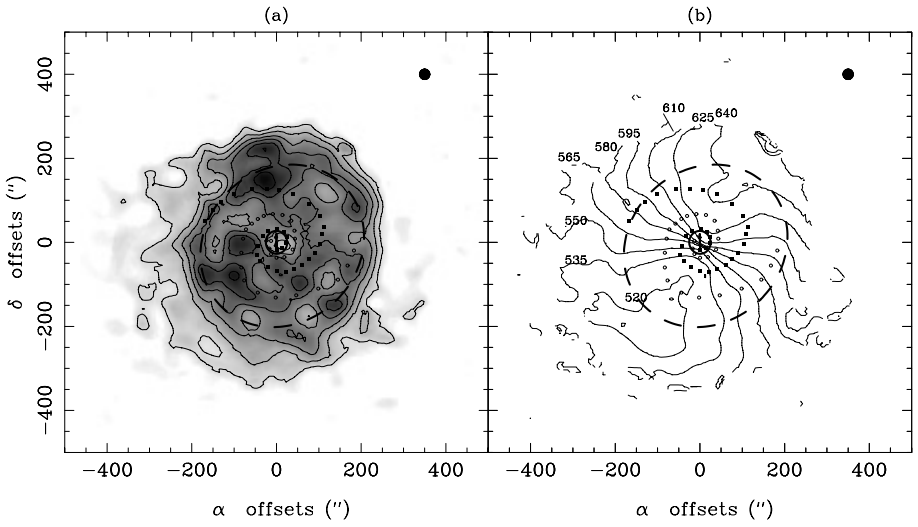

Fig. 8. a Map of the HI column density distribution in NGC 3344. The contour interval is 1.9×10^{20} atoms cm^{-2}, and the first contour corresponds to 1.9×10^{20} atoms cm^{-2}. **b** Map of the first-order moment of the radial velocity field. The numbers indicate heliocentric velocities in km s^{-1}. Synthesized beam = 60.″0 × 60.″0 ($\alpha \times \delta$). We have outlined the oval, the inner and outer rings are as well as the spiral structure.

part hook pronouncedly toward the south for the whole velocity range. From v_{hel} = 524 to 540.5 km s^{-1} this bending takes the form of an arc connecting the two outer parts of the emission (radii $\sim$ 5.′4). A similar behaviour is detected in the convolved maps at v_{hel} between 606 and 623 km s^{-1} but at smaller radii ($\sim$ 4.′8). The north-east half of the galaxy is also perturbed for the lowest velocities, showing a more regular behaviour for velocities larger than 570 km s^{-1}.

For an overall view of the HI emission we show in Fig. 8a the HI column density distribution as both a gray scale and contours. It was obtained after smoothing the channel maps with a gaussian tapering function leading to a beam size of 60″ × 60″. Then the channel maps were manually "blotted" to exclude contributions of sky where no emission was detected, while pixels where the emission intensity exceeds the r.m.s. noise (1σ) were added up. In the figure we also show the orientation of the bar, the outline of the inner and outer rings, and the spiral structure as seen in the B band. The azimuthally averaged radial distribution of the HI column density is shown in Fig. 4d. It has been obtained by averaging the two-dimensional HI distribution (Fig. 8a) in elliptical rings using the geometrical parameters obtained from the HI velocity field (see Sect. 3.4). For the radii where the optical emission has been detected we have checked that the adoption of the geometrical parameters corresponding to the R isophotes does not change significantly the profile. Therefore direct comparison with the other panels in Fig. 4 is possible.

As already noted in the individual channel maps, at low levels the atomic gas is more extended to the SE part of the galaxy (from p.a. 50° to 245°). The atomic gas measured at 1.5×10^{20} cm^{-2} (310″) extends 34% more than the optical dimension (R_{25} = 210.″6 in B band) to the NW and 60% more to the SE. This extension occurs in a direction similar to that of the isophotal centers of the optical emission (Fig. 6). The bar and inner ring area are relatively devoid of HI, which falls to $\sim$ 40% of the peak HI surface intensity for the central 25″. The CO emission does not seem to fill uniformly this hole, but covers mostly the region of the inner ring (Braine & Combes 1993). There is a good correspondence between portions of the spiral arms and HI peaks. In particular the highest column density in the HI distribution, 1.2×10^{21} cm^{-2} occurs at a very bright complex in B (22.6 mg/(″)^2 located at $\sim$ (–8,158)″. The arms can be traced beyond their optical emission, especially the northern one. The counterpart of this arm to the south shows lower column densities. Some of the gas associated to this arm might have been displaced into the SE extension. The outer ring is detected in HI as several clumps. The radial distribution of the HI surface density (Fig. 4d) reflects several of these features. Thus it shows very clearly the central HI depression, and has some humps corresponding to the different HI clumps seen in Fig. 8a and coming from the spiral arms. The emission from $\sim$ 180″ to 220″ is associated to the outer ring and the atomic gas does not show enhanced densities there with respect to the other HI clumps. The HI emission from radii between 300″ and 360″ originates from the asymmetric extension of NGC 3344 to the SE.

The global HI profile is shown in Fig. 9, and was obtained by integrating the flux density in each channel map over an area containing the line emission. It shows a typical two horned shape. The emission is stronger at 528 km s^{-1} ($S_\nu \sim$ 1.4 Jy) than at its symmetrical velocity, 648 km s^{-1}, ($S_\nu \sim$ 1.3 Jy). This is due to the excess emission associated with the southeastern HI extension. The global flux is 10% lower than the one measured by Staveley-Smith & Davies (1987) with single dish HI observations (Table 3), most of the emission missing at the velocity corresponding to the minor axis direction. The missing HI is at low level and extended, so the asymmetries would persist when all gas taken into account. This is supported by the asymmetry still visible in the single dish spectrum. The detected HI mass estimated from this profile is 2.0×10^9 $M_\odot$.

3.3. HI velocity field

The velocity field of NGC 3344 is shown in Fig. 8b where the characteristics already visible in the channel maps can be recognized. The inner parts correspond reasonably well to a disk

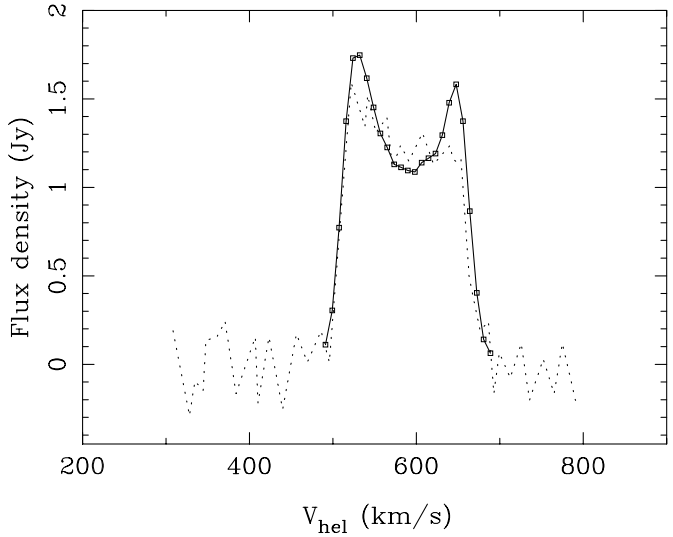

Fig. 9. HI flux density of NGC 3344 as a function of heliocentric velocity. The HI profile from Staveley-Smith & Davies (1987) is plotted with a dotted line for comparison.

Table 3. Derived Parameters

H_I flux[a]	178.7 Jy km s^{-1}
H_I flux[b]	199.1 Jy km s^{-1}
M^a_{HI}	2.0×10^9 M$_\odot$
M^b_{HI}	2.2×10^9 M$_\odot$
$M_{HI}/L^{0\,a}_B$	0.16
$M_{\rm bulge}$ (out to 7.1 kpc) [a]	2.0×10^8 M$_\odot$
$M_{\rm disk}$ (out to 7.1 kpc) [a]	1.6×10^{10} M$_\odot$
$M_{\rm gas}$ (out to 7.1 kpc) [a]	1.7×10^9 M$_\odot$
$M_{\rm halo}$ (out to 7.1 kpc) [a]	2.7×10^{10} M$_\odot$

[a] This paper
[b] Staveley-Smith & Davies (1987).

in regular rotation, and part of the kinks correlate with the HI clumps associated to the spiral arms. But most of the perturbations for the largest radii are characteristic of a warped disk (cf. e.g. Bosma 1981). A clear asymmetry exists between the approaching and receding part of the disk, especially to the SE where the warp seems to set in very abruptly, leading to pronounced hooks in the isovelocity contours.

We have tried to model the velocity field of NGC 3344 fitting a tilted ring model (see Begeman 1987; the ROTCUR task in Gipsy). For the reasons explained above this is not straightforward, and it is further complicated by the fact that the warp starts at different radii on the minor axis direction (R $\sim$ 200″) than on the major axis one (R $\sim$ 250″). Therefore we have tried different combinations of the inclination, position angle and rotational velocity as we describe below.

In all cases the galaxy has been divided into concentric rings, each of them with a width of 10″ along the major axis and a central position fixed to the optical center (Table 1). Points within a sector of $\pm$ 30° from the minor axis were excluded from the fits. We analysed independently the approaching and receding parts of the galaxy and also calculated a rotation curve by averaging both sides. The expansion velocities were set to 0 and the systemic velocity initially fixed to the central velocity of the HI spectrum at half maximum intensity (586.6 km s^{-1}). Allowing the systemic velocity to vary freely leads to a very similar value of 586.8 $\pm$ 0.4 km s^{-1} which has then been adopted.

Convergence was not reached in any case for radii $<$ 50″ due to the gas deficiency there. First we have allowed inclination and position angle to variate freely, but the errors for the inclination and rotation velocity were large for all radii. Next we have assumed a constant inclination for all radii equal to a value of 25.5° as obtained from the optical photometry, resulting in the position angles plotted in Fig. 10a, where they are plotted twice with a 360° shift in order to allow comparison with the optical values. The abrupt change in the position angle for radii larger than 200″ is well reproduced as can bee seen with more detail in Fig. 10b, while the rotation curve falls rapidly in the outer parts (Fig. 10c).

The fall in the rotation curve in the outer parts might be directly related to us keeping the inclination constant. Since it seems more likely that the inclination of the outer HI layer changes as well, we now adopt a flat rotation curve in the outer parts. Different combinations of the position angle and inclination as function of radii were then tested by modelling the galaxy with the task GALMOD in Gipsy.

First, we keep the rapid change in position angle for the most pronouncedly warped parts of NGC 3344, as given above by ROTCUR. We then find a model defined by the geometrical parameters plotted in Fig. 11a and b, whose corresponding velocity field is shown in Fig. 12a. However, in this case unreasonable values for the inclination and rotational velocity (Fig. 11c) are obtained. This is due to the inhomogeneous behaviour of the velocity field, which shows varying degrees of twisting and at different distances from the center.

A better overall description is obtained when we vary both p.a., and inclination more smoothly, while keeping the rotation curve constant. This is indicated by the parameters plotted in Fig. 13 a and b, and the obtained velocity field (Fig. 12b). The resulting rotation curve after analysing the model with ROTCUR is plotted in Fig. 13c. The position angle for the inner parts ($<$ 150″) showed a very stable value for all tested models, with a mean value of –23.9° $\pm$ 0.7° in the range 45″ - 155″, similar to the one obtained from our optical photometry (–20.2°). Since the HI velocity field gives a more precise determination for a larger range of radii, we will adopt for the position angle a value of –23.9°.

4. Discussion

4.1. The small bar and the rings

We have fitted an exponential disk component to the outer parts of the R profile of NGC 3344, obtaining μ_d = 19.7 mag (arcsec)$^{-2}$ and r_d = 43″. The residuals were poorly fitted by a de Vaucouleurs law leaving a residual of the order of 20.2

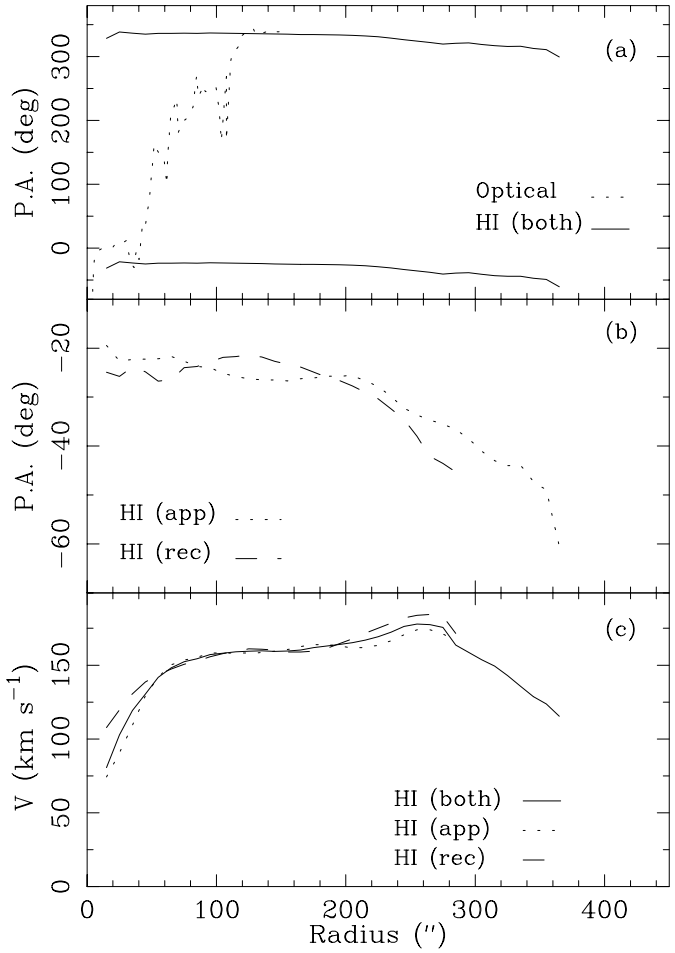

Fig. 10. **a** Position angle of NGC 3344 obtained from the fitting of a tilted ring model to both sides of the HI velocity field (Sect. 3.3.) is shown by a solid line. It is repeated with a 360° shift in order to allow comparison with the isophotal fitting of the optical R image (see also Fig. 4b), shown by a dotted line. Angles are measured from North to East. **b** The same as in **a** but obtained separately for the approaching (solid line) and receding (dashed line) halves. The HI emission is less extended for the receding half (Fig. 8) and therefore the p.a. could not be determined to the same extent as the approaching one. **c** HI rotation velocity derived from the HI velocity field assuming circular motions. The solid line correspond to the curve derived for both sides of the galaxy. Dashed and dotted ones correspond respectively to rotation curves derived independently from the receding and the approaching side.

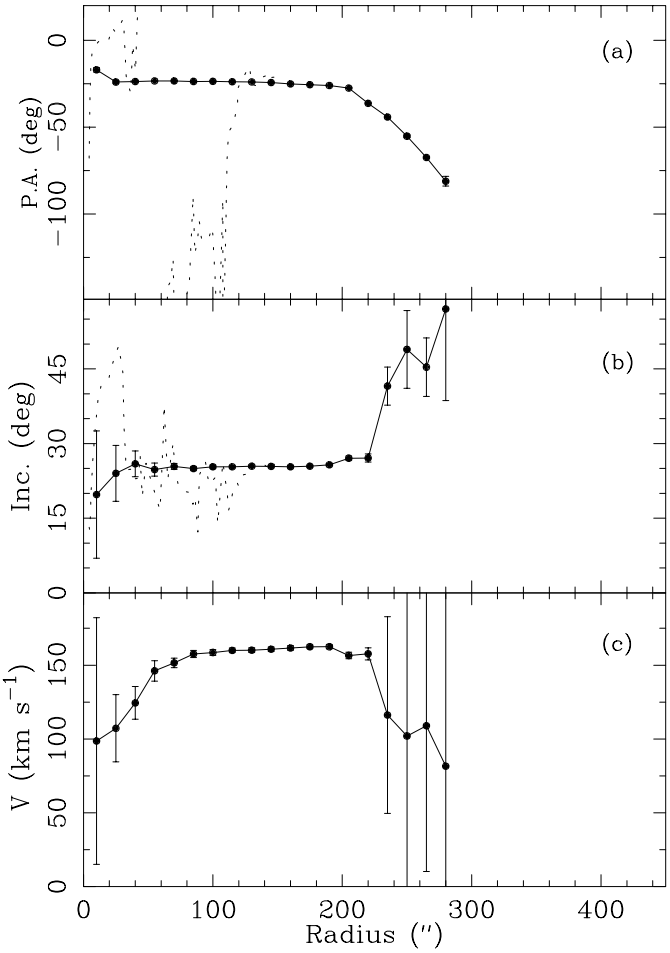

Fig. 11a–c. Position angle (**a**) and inclination (**b**) of NGC 3344 used to model the galaxy channel maps, and corresponding to the velocity field shown in Fig. 12 a. The rapid change in position angle visible in the observed channel maps is well reproduced, although unrealistic values are obtained for the inclination, as well as for the rotational velocity plotted in **c**. The dotted lines correspond to the isophotal fitting of the optical R image (Fig. 4b). Angles are measured from North to East.

mag (arcsec)$^{-2}$. An exponential fit was more appropriate, with residuals reduced to 20.7 mag (arcsec)$^{-2}$. Cuts of the R image along the major and minor axis of the bar show that this exponential behavior is not axisymmetric but follows the bar shape. This profile is characteristic for a late type bar (Elmegreen et al. 1996b; Elmegreen & Elmegreen 1985) and such classification is supported by the lack of isophotal twist (Elmegreen et al. 1996a) as well as its characteristic size (R_{bar}/R_{25} = 0.1). Therefore it suggests that the bulge component is quite small and the inner parts of the galaxy are dominated by the bar component. It was probably mistaken as the bulge leading to an Sbc classification for NGC 3344, while an Sc/Sd morphology seems here more appropriate. Such a later classification removes the slight puzzle posed by the strong metallicity gradient, as determined by Mc Call et al. (1981).

Both the inner and outer ring show similar blue colours (Sect. 3, Table 2) although a higher HI surface density is associated to the outer one (Fig. 4). Since none of the rings are prominent in the I band, young stars constitute the dominant component of both rings. Less than 1% of the HI mass is associated to the inner ring, and roughly 20% to the outer one, although it is quite possible that the inner ring contains molecular gas. Deprojection of the galaxy with p.a. = -23.9° and i = 25.5° gives for the inner ring a size of 29.″8 with an axial ratio of 0.93 and a p.a. of 36°, being well centered in the optical maximum of the image. The outer ring would have an intrinsic a size of 217.″2 with an axial ratio of 0.92 and a p.a. of -3.9°, being offset to the east by $\sim 18''$.

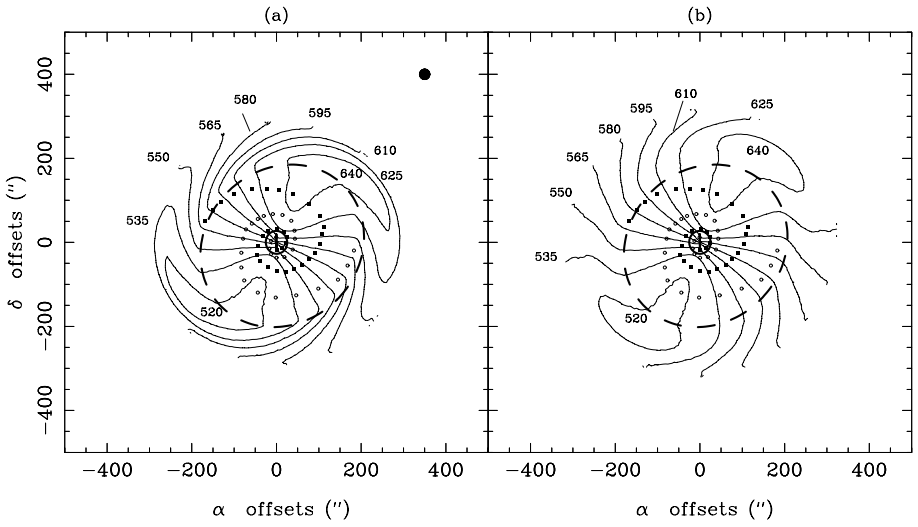

Fig. 12a and b. Map of the first-order moment of the modeled channel maps obtained with the geometrical parameters plotted in Fig. 11 for **a** and Fig. 13 for **b**. The numbers indicate heliocentric velocities in km s^{-1}. We have outlined the oval, the inner and outer rings are as well as the spiral structure.

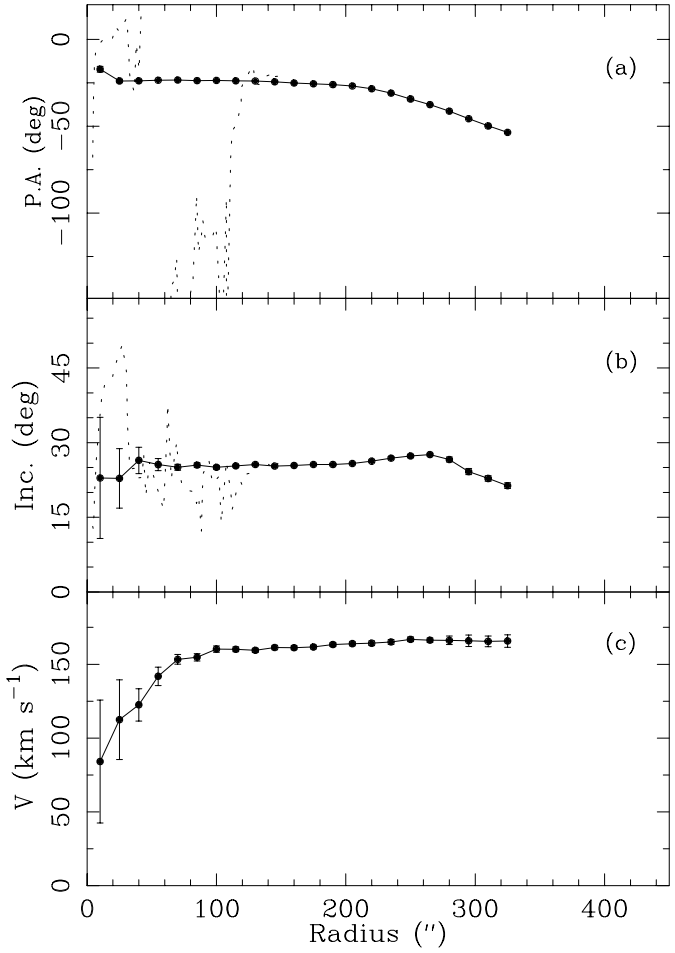

Fig. 13. a Position angle and **b** inclination of NGC 3344 used to model the galaxy channel maps, and corresponding to the velocity field shown in Fig. 12 b. The derived rotation curve is plotted in **c**. A better overall description is obtained with these parameters than with those shown in Fig. 11 a and b, although the latter give a better reproduction of the abrupt change in position angle. The dotted lines correspond to the result for the isophotal fitting of the optical R image (Fig. 4b). Angles are measured from North to East.

4.2. Rotation curve and mass model

We have also constructed a rotation curve based on our optical data. These data are shown in Fig. 14, together with the rotation curve determined from the radio data. As can be seen, there is good agreement between the two sets of data for radii larger than 55″, while the effect of beam smoothing on the radio rotation curve is important in the inner parts, due to the large and elongated beam. We also note that in the very center the optical data show a rather large scatter. In fact, in the single position-velocity data we find weak indications of counter rotation in the very central parts (radii less than 5″), but unfortunately our data do not have sufficient spatial resolution to establish this clearly.

To compute a mass model, we combined the optical and radio data into one curve, by adopting the optical data out to 75″ and the HI data for larger radii. Beyond 200″, we arbitrarily assume that the rotation curve remains constant, even though the evidence is based only on our modeling for the warp (cf. Fig. 13c). The result is summarized in Table 4, where the errors reflect the errors in the mean. The last entry in Table 4 has been repeated for radii up to 365″ in the calculation of the mass models.

We have calculated a mass model for this galaxy, using the precepts discussed in Athanassoula et al. (1987), using the I-band radial luminosity profile, and assuming a maximum disk. The resulting curves are shown in Fig. 15. The computed mass-to-light ratio for the bulge is 4.0, and for the disk is 4.0 (uncorrected for internal extinction). It can be seen that the fit is not very satisfactory in the inner parts. This is due partly to the presence of the small bulge and bar, which can not be very well modeled assuming circular motions only, and probably also due to colour gradients in the disk. The core radius of the halo is 7.0 kpc and its central density 0.028 $M_\odot$ pc^{-3}. Thus the ratio of halo core radius to optical radius is about 0.8.

Due to the uncertainties in the inner parts, it is very difficult to derive the curve of the epicyclic frequency κ, which is needed for calculating the curves of $\Omega \pm \kappa/2$. Hence we cannot determine whether e.g. the inner ring corresponds to an inner

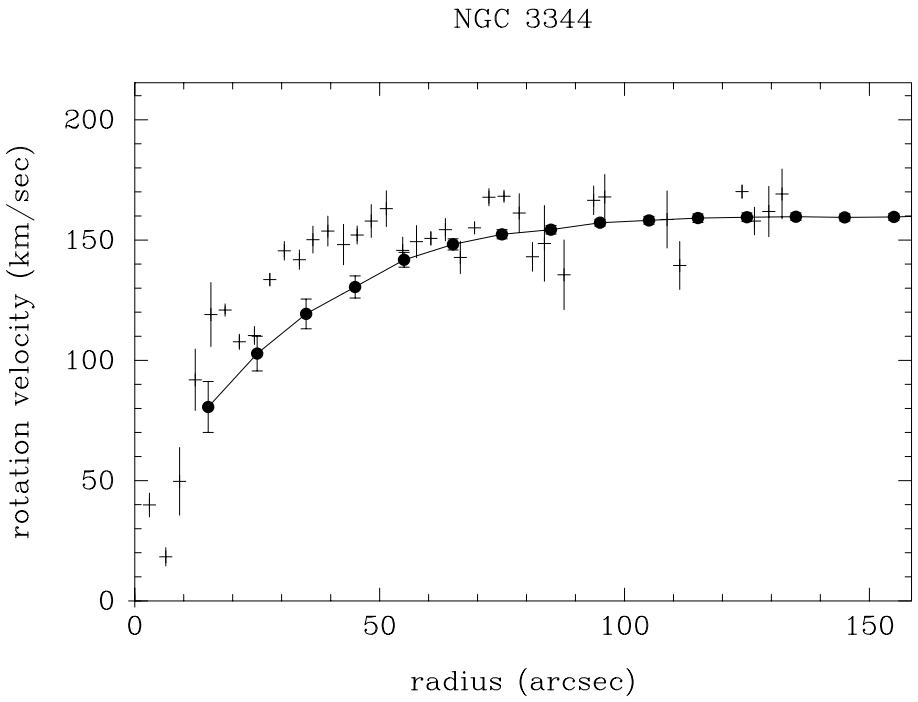

Fig. 14. Comparison of the optical rotation curve (crosses), and the HI rotation curves (filled dots).

Lindblad resonance, while for the same pattern speed the outer pseudo ring then corresponds to the outer Lindblad resonance.

5. Concluding remarks

We embarked on this study of the galaxy NGC 3344 to seek the explanation for the presence of the inner and outer ring, hoping to link them together as resonance features set up by an underlying structural pattern, for us to discover, as we managed to do for NGC 7217 (Verdes Montenegro et al. 1995) and NGC 6015 (Verdes Montenegro et al. 1997). This has not proven possible due to the complexity of the galaxy.

The inner parts are dominated by a small bulge, a small bar, and an inner ring surrounding it, at whose radius starts a prominent spiral structure. In the outer parts, where the main spiral structure stops, there is an outer pseudo-ring, which is not centered on the nucleus, and beyond this the HI layer shows a strong and asymmetric warp. All these complexities, and in particular the asymmetries, prevent us from deriving correctly the axisymmetric quantities we need to know in order to explore the geometric positions of the resonances.

Several of the complex features can be linked together. Other galaxies exist which have small bar in the central parts, and an inner ring around it sharing the same orientation of the bar major axis, though this phenomenon occurs mainly in later type galaxies. Even so, it is clear that the outer ring cannot be considered as the outer Lindblad resonance of the bar, since its location is far beyond the radius we expect for the bar's outer Lindblad resonance if the standard picture of bars ending roughly at the corotation radius is adopted.

We could also point to a possible link between the outer ring, the strong spiral structure, and the warp in the HI layer, as a manifestation of the warp generation mechanism proposed by Masset & Tagger (1997), who suggest a coupling of a spiral wave and two warp waves at the location of the outer Lindblad resonance of the spiral. However, we cannot easily link up the perturbations in the inner parts with those in the outer parts, and thus arrive at a global picture explaining the formation and properties of all these structures at once.

Table 4. Rotation curve (optical left, radio right)

Radius (arcsec)	Rot. velocity (km/s)	r.m.s. error (km/s)	Radius (arcsec)	Rot. velocity (km/s)	r.m.s. error (km/s)
3.0	39.9	4.9	15.0	80.6	10.6
6.3	18.3	3.8	25.0	102.8	7.2
9.2	49.7	14.1	35.0	119.3	6.2
12.4	91.9	12.7	45.0	130.5	4.6
15.6	119.0	13.3	55.0	141.8	3.1
18.5	120.9	1.7	65.0	148.2	2.3
21.4	107.7	3.1	75.0	152.4	1.9
24.4	110.3	3.7	85.0	154.3	1.8
27.6	133.6	2.7	95.0	157.2	1.4
30.5	145.5	3.9	105.0	158.2	1.6
33.6	141.8	4.0	115.0	159.1	1.8
36.4	150.2	5.6	125.0	159.5	1.8
39.4	153.8	6.2	135.0	159.7	1.6
42.6	148.1	8.4	145.0	159.4	1.5
45.4	152.1	3.7	155.0	159.6	1.4
48.3	157.9	6.8	165.0	160.3	1.4
51.4	163.0	7.4	175.0	161.9	1.5
54.7	145.7	5.5	185.0	163.0	1.5
57.5	149.3	6.7	195.0	164.0	1.6
60.5	150.7	2.9	205.0	165.0	2.2
63.4	154.3	4.6	215.0	165.0	5.0

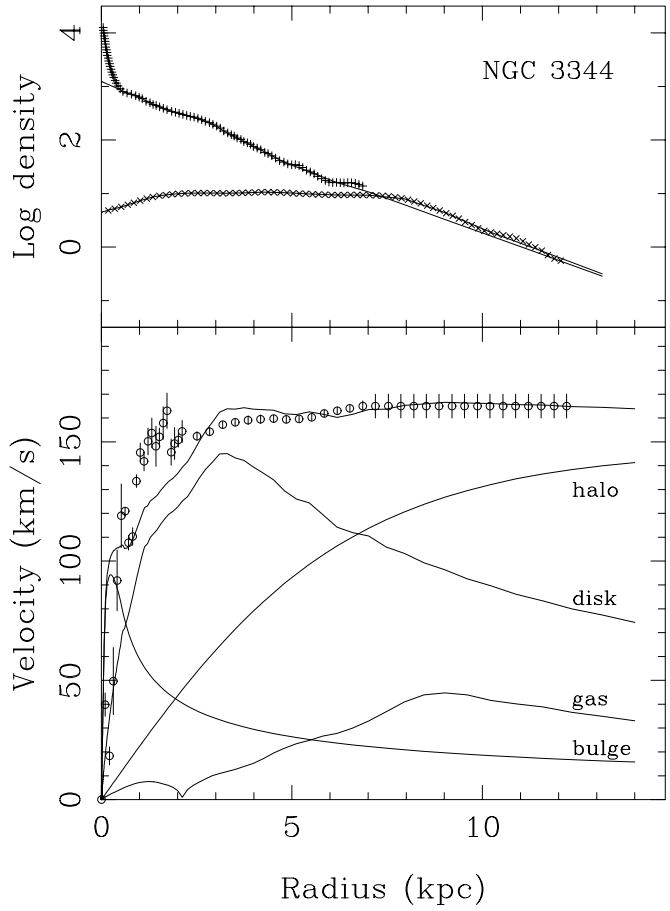

Fig. 15. Composite bulge/disk/gas/halo mass model for NGC 3344. In the top panel the radial distributions of the stellar (pluses) and gas (crosses) components are given in units of $M_\odot$ pc^{-2}. In the bottom panel the rotation curves are shown for each of the components (labelled curves), the best fitting total curve, and the adopted observed rotation curve (circles with error bars).

The relative isolation of the galaxy (no bright nearby companion) poses a further problem: are all the remarkable features in this galaxy formed intrinsically and long lived? The strong abundance gradient found by McCall et al. (1981), more reminiscent of an Sc galaxy, should also be explained. Instead of relying on intrinsic mechanisms to explain all these phenomena, we can envisage that this galaxy underwent a recent accretion event which modified its morphology. Its basic structure is more like that of a giant Sc galaxy, but with morphological details which are a bit unusual (presence of an outer ring, presence of a small bar of limited radial extent, a yet to be confirmed hint in our data that the bulge does not rotate the same way as the disk). It could be that at least the outer ring is a transient structure set up by this event, thereby explaining the relative rarity of such a feature in average late type spirals.

Acknowledgements. LV–M acknowledges the hospitality and financial support of the Observatoire de Marseille, where part of this work was carried out, and helpful discussions with Dr. A. del Olmo. LV–M is partially supported by DGICYT (Spain) Grant PB96-0921 and Junta de Andalucía (Spain). We thank the referee, Dr. P. Appleton, for helpful comments, which improved the presentation of our results.

References

Athanassoula E., 1996, In: Buta R., Crocker D., Elmegreen B.G. (eds.) Barred galaxies. IAU Coll. 157, ASP Conf. Series 91, p. 309
Athanassoula E., Bosma A., Crézé M., Schwarz M.P., 1982, A&A 107, 101
Athanassoula E., Bosma A., Papaioannou S., 1987, A&A 179, 23
Athanassoula E., Bosma A., Guivarch B., Verdes-Montenegro, L., 1996, In: Bender R., Davies R.L. (eds.) New Light on Galaxy evolution. IAU Symp. 171, Kluwer, Dordrecht, p. 339
Begeman K., 1987, Ph.D. Thesis, University of Groningen
Bos A., Raimond E., van Someren Greve H.W., 1981, A&A 98, 251
Bosma A., 1981, AJ 86, 1825
Braine J., Combes F., Casoli F., et al., 1993, A&AS 97, 887
Briggs F.H., 1990, ApJ 352, 15
Burstein D., Heiles C., 1984, ApJS 54, 33
Buta R., 1986, ApJS 61, 631
Buta R., 1995, ApJS 96, 39
Buta R., Crocker D.A., 1991, AJ 102, 1715
Considère S., Athanassoula E., 1988, A&AS 76, 365
Corbelli E., Schneider S.E., Salpeter E.E., 1989, AJ 97, 390
De Vaucouleurs G., Buta R., 1980, AJ 85, 637
De Vaucouleurs G., De Vaucouleurs A., Corwin H.G., 1976, The Second Reference Catalog of Bright Galaxies. University of Texas Press, Austin
De Vaucouleurs G., de Vaucouleurs A., Corwin H.G., et al., 1991, Third Reference Catalogue of Bright Galaxies. Springer, Berlin
Elmegreen B.G., 1996, In: Buta R., Crocker D., Elmegreen B. (eds.) Barred Galaxies. IAU Colloquium 157, ASP, San Francisco, p. 197
Elmegreen D.M., Elmegreen B.G., 1984, ApJS 54, 127
Elmegreen B.G., Elmegreen D.M., 1985, ApJ 288, 438
Elmegreen B.G., Elmegreen D.M., Chromey F.R., Hasselbacher D.A., Bissell B.A., 1996a, AJ 111, 1880
Elmegreen B.G., Elmegreen D.M., Chromey F.R., Hasselbacher D.A., Bissell B.A., 1996b, AJ 111, 2233
Frei Z., Guhathakurta P., Gunn J.E., Tyson J.A., 1996, AJ 111, 174
García-Gómez C., Athanassoula E., 1991, A&AS 89, 159
Grosbøl P.J., 1985, A&AS 60, 261
Gullixson C.A., Boeshaar P.C., Tyson J.A., Seitzer P., 1995, ApJS 99, 281
Maoz D., Filippenko A.V., Ho L.C., et al., 1996, ApJS 107, 215
Masset F., Tagger M., 1997, A&A 318, 747
Martin P., 1995, AJ 109, 2428
Mc Call M.L., Rybski P., Shields G.A., 1981, PASP 93, 273
Merrifield M., Kuijken K., 1994, ApJ 432, 575
Patsis P.A., Hiotelis N., Contopoulos G., Grosbøl P., 1994, A&A 286, 46
Sandage A., Bedke J., 1988, Atlas of galaxies. Useful for measuring the cosmological distance scale. NASA SP, NASA, Washington
Savage B.D., Mathis J.S., 1979, ARA&A 17, 73
Schwarz M.P., 1981, ApJ 247, 77
Schwarz M.P., 1984a, A&A 133, 222
Schwarz M.P., 1984b, MNRAS 209, 93
Schwarz M.P., 1984c, Proc. Astr. Soc. Australia 5, 464
Schwarz M.P., 1985, MNRAS 212, 677
Staveley-Smith L., Davies R.D., 1987, MNRAS 224, 953
Verdes-Montenegro L., Bosma A., Athanassoula E., 1995, A&A 300, 65
Verdes-Montenegro L., Bosma A., Athanassoula E., 1997, A&A 321, 754